JOURNAL OF THERMOPHYSICS AND HEAT TRANSFER
Vol. 20, No. 3, July–September 2006

Transient Coupled Heat Transfer Inside a Scattering Medium with Graded Refractive Index

He-Ping Tan* and Hong-Liang Yi†
Harbin Institute of Technology, 150001 Harbin, People's Republic of China
Jian-Feng Luo‡
National University of Defense Technology, 410073 Changsha, People's Republic of China
and
Hao-Chun Zhang§
Harbin Institute of Technology, 150001 Harbin, People's Republic of China

Transient heat transfer of coupled radiation and conduction within a semitransparent parallel plane slab of absorbing–emitting–scattering gray medium with graded index is investigated. The refractive index of the medium varies continuously along the slab thickness, and both boundary surfaces are specular and semitransparent. The medium is discretized into a number of sublayers with a constant refractive index in each, in which the radiative transfer is numerically simulated using a multilayer radiative transfer model. The multilayer model is developed using a ray-tracing method based on a zonal method. Comparison of present results with previous research shows excellent agreement, which helps to verify the validity of the multilayer radiative transfer model of a medium with a graded refractive index. Effects of optical thickness, scattering albedo, and gradient of refractive index on transient thermal behavior are examined for a medium with nonlinear refractive index distributions. It is found that temperature peaks also appear in the inner regions of a graded refractive index medium with two semitransparent surfaces subjected to external radiation even though there is no convection cooling on the surfaces and the absorbing coefficient (or extinction coefficient) is spatially uniform in the medium.

Nomenclature

b_1, b_2	=	surface or interface, used to define multilayer radiative intensity quotient transfer function
C	=	unit heat capacity, $\mathrm{Jm^{-3}K^{-1}}$
$\boldsymbol{F}$	=	radiative intensity quotient transfer function of a single-layer model
$f(\theta)$	=	transfer function of the total intensity quotient absorbed by V_{J_b} to that emitted by V_{I_a}
$\boldsymbol{H}$	=	radiative intensity quotient transfer function of a multilayer model
H_1, H_2	=	convection–radiation parameters, $h_1/\sigma T_r^3$ and $h_2/\sigma T_r^3$, respectively
h_1, h_2	=	convective heat transfer coefficients at surfaces S_1 and S_2, respectively, $\mathrm{Wm^{-2}K^{-1}}$
I_b, J_b	=	the Ith node and Jth node in the bth sublayer, respectively
k	=	thermal conductivity of a slab, $\mathrm{Wm^{-1}K^{-1}}$
k_b	=	thermal conductivity of the bth sublayer of a slab, $\mathrm{Wm^{-1}K^{-1}}$
k_{ie}	=	harmonic mean thermal conductivity at interface ie of control volume i
k_{iw}	=	harmonic mean thermal conductivity at interface iw of control volume i
L	=	thickness of a slab, $L_1 + L_2 + \cdots + L_n$, m
L_b	=	thickness of the bth sublayer, m
M_b	=	number of control volumes of the bth sublayer
M_t	=	total number of control volumes of a composite, $M_1 + M_2 + \cdots + M_n$
N_b	=	conduction–radiation parameter of the bth sublayer of a slab, $k_b/(4\sigma T_r^3 L)$
N_{ie}, N_{iw}	=	conduction–radiation parameters, $k_{ie}/(4\sigma T_r^3 L)$ and $k_{iw}/(4\sigma T_r^3 L)$, respectively
$N_{\text{Ref. 34}}$	=	conduction–radiation parameter defined according to Ref. 34 as $k\kappa/(4\sigma n_R^2 T_R^3)$
n	=	total number of sublayers of a multilayer radiative transfer model
$n(X)$	=	refractive index of the considered slab, continually varying with dimensionless coordinate X
n_b	=	refractive index of the bth sublayer
n_c, n_s	=	refractive index values at the center position and the surface of a slab, respectively
n_m	=	refractive index of the mth element
n_R	=	reference refractive index, specified as 1.5, given in Ref. 34
n_0, n_{n+1}	=	refractive indexes of surroundings (equal to the refractive index of air n_g)
n_i'	=	refractive index of the ith control volume. When $i \le M_1$, $n_i' = n_1$; when $M_1 + \cdots + M_{b-1} < i \le M_1 + \cdots + M_b$, $n_i' = n_b$
P_b	=	side of interface P_b facing towards the bth sublayer
$P_{b'}$	=	side of interface P_b facing towards the $(b+1)$th sublayer
$\overline{P_b}$	=	interface between the bth sublayer and $(b+1)$th sublayer
P_m	=	side of interface P_m facing towards the mth sublayer (see Fig. 2)
$P_{m'}$	=	side of interface P_m facing towards the $(m+1)$th sublayer (see Fig. 2)
$\overline{P_m}$	=	interface between the mth sublayer and $(m+1)$th sublayer (see Fig. 2)

Received 28 January 2005; revision received 8 November 2005; accepted for publication 27 November 2005.

*Professor, School of Energy Science and Engineering, 92 West Dazhi Street; tanheping77@yahoo.com.cn.
†Ph.D. Candidate, School of Energy Science and Engineering, 92 West Dazhi Street; hongliang_yi@yahoo.com.cn.
‡Associate Professor, School of Science; luo-jianfeng@263.net.
§Ph.D. Candidate, School of Energy Science and Engineering, 92 West Dazhi Street; hczhang@hit.edu.cn.

q = heat flux, Wm^{-2}
q^{cd}, q^{r} = thermal conductive and radiative heat fluxes, respectively, W m^{-2}
q^{*} = dimensionless heat flux, $q/(4\sigma T_r^4)$
S_u, S_v = black surrounding surfaces, $u, v = -\infty$ or $+\infty$
(S_uS_v), $[S_uS_v]$ = ratio of radiative energy arriving at S_v to that emitted from S_u for a nonscattering and scattering medium, respectively
(S_uV_j), $[S_uV_j]$ = ratio of radiative energy arriving at V_j to that emitted from S_u for a nonscattering and scattering medium, respectively
S_1, S_2 = boundary surfaces of a slab
$S_{-\infty}$, $S_{+\infty}$ = the left and right black surfaces representing surroundings
Sc_i = constant part of Φ_i^{r*}
Sp_i = modulus of Θ_i, $S_{pi} \le 0$
T = temperature, K
T_{g1}, T_{g2} = gas temperatures for convection at $x = 0$ and L respectively, K
T_i = temperature at control-volume i
T_R = reference temperature, $(T_{+\infty} + T_{-\infty})/2$, defined in Ref. 34
T_r = reference temperature, K
T_{S_1}, T_{S_2} = temperatures of boundary surfaces S_1 and S_2, respectively, K
T_0 = uniform initial temperature, K
$T_{-\infty}$, $T_{+\infty}$ = temperatures of black surfaces, $S_{-\infty}$ and $S_{+\infty}$, respectively, K
t = physical time, s
t^{*} = dimensionless time, $4\sigma T_r^3 t/(CL)$
V_i = the ith control volume, $i = M_1 + \cdots + M_{b-1} + I_b$
V_{I_b} = the Ith control volume of the bth sublayer, $I = 1$ to M_b
(V_iV_j), $[V_iV_j]$ = ratios of radiative energy arriving at V_j to that emitted from V_i for a nonscattering and scattering medium, respectively
(V_jS_u), $[V_jS_u]$ = ratio of radiative energy arriving at S_u to that emitted from V_j for a nonscattering and scattering medium, respectively
X = dimensionless coordinate in direction across a slab, $X = x/L$
x = coordinate in direction across a slab, m
x_i, y_i, z_i, w_i, x_i', w_i', z_i' = geometrical progressions used in tracing radiative intensity (see Fig. 3)
y, z = quotients of the radiative intensity emitted by V_{l_a} finally reaching P_{b-1} and $P_{b'}$, respectively [see Eqs. (10), (11), and Fig. 3]
β_2, β_3, β_4, β_5 = common ratios of infinite geometric progressions [see Eqs. (7), (8), (10), and (11)]
$\Gamma(\theta)$ = transfer quotient of radiative intensity to control volume or surface
$\gamma(\theta)_{b,b-1}$ = transmissivity of radiative intensity propagating from sublayer b to sublayer $b-1$
$\gamma(\theta)_{bo}$ = transmissivity of radiative intensity propagating from sublayer b to sublayer o at angle θ, $1 - \rho(\theta)_{bo}$
Δm = number of sublayers in a multilayer model (see Fig. 2)
Δt = time interval, s
Δt^{*} = dimensionless time interval, $4\sigma T_r^3 \Delta t/(CL)$
ΔX = dimensionless control volume thickness, $\Delta x/L$
Δx = control volume thickness, m
η_i = $1 - \omega_t'$
Θ_{g1}, Θ_{g2} = gas dimensionless temperatures for convection T_{g1}/T_r and T_{g2}/T_r, respectively
Θ_i = dimensionless temperature of control volume i, T_i/T_r
Θ_{S_1}, Θ_{S_2} = dimensionless temperatures of boundary surfaces, T_{S_1}/T_r and T_{S_2}/T_r, respectively
Θ_0 = uniform dimensionless initial temperature, T_0/T_r
$\Theta_{-\infty}$, $\Theta_{+\infty}$ = dimensionless temperatures of black surfaces, $T_{-\infty}/T_r$ and $T_{+\infty}/T_r$, respectively
θ = incident angle of the mth element, rad
θ_b = refractive angle in sublayer bth, arcsin $(\sin\theta n_m/n_b)$, rad
θ_{ba} = arrangement of critical angles, θ_{ba}', from small to big, where $a = 0$ to $n+1$
θ_{ba}' = critical angle. If $n_b > n_a$, θ_{ba}', $= \arcsin(n_a/n_b)$, else $\theta_{ba}' = \pi/2$, where $a = 0$ to $n+1$
κ = extinction coefficient of a slab, m^{-1}
κ_b = extinction coefficient of the bth sublayer of a slab, m^{-1}
μ_b = $\cos\theta_b$
ρ_b = density of the bth sublayer of a slab, kg m^{-3}
$\rho_{m,m+1}$ = reflectivity from sublayer m to sublayer $m+1$ (see Fig. 2)
$\rho(\theta)_{bo}$ = reflectivity from sublayer b to sublayer o at angle θ
σ = Stefan–Boltzmann constant, $\mathrm{Wm}^{-2}\mathrm{K}^{-4}$
τ = optical thickness of a slab, κL
τ_b = optical thickness of sublayer bth, $\kappa_b L_b$
Φ_i^r = radiative heat source term of control volume i, Wm^{-2}
Φ_i^{r*} = dimensionless radiative heat source term of control volume i, $\Phi_i^r/(4\sigma T_r^4)$
φ_o = refractive angle in the oth sublayer, arcsin $(n_b/n_0 \sin\theta_b)$
ω = scattering albedo of a slab
ω_b = scattering albedo of the bth sublayer
ω_t' = scattering albedo of the ith control volume. When $i \le M_1$, $\omega_i' = \omega_1$; when $M_1 + \cdots + M_{b-1} < i \le M_1 + \cdots + M_b$, where $1 < b \le n$, $\omega_i' = \omega_b$

Subscripts

a = sublayer index, $a = 1$ to n; absorption quotient
$a1_b$ = surface, interface, or control volume of the bth sublayer, used to define one-layer radiative intensity quotient transfer function
b = sublayer index, $b = 1$ to n
bo = radiative intensity propagating from sublayer b to sublayer o
$b{-}n$ = a multilayer model composed of the layers from the bth sublayer to the nth sublayer
c = the cth sublayer, either sublayer b or o
g = gas (air)
I_a, J_b = the Ith node or control volume in the ath sublayer and the Jth node or control volume in the bth sublayer
i = the ith control volume
ie, iw = the left and right interfaces of the ith control volume
k = relative to the kth spectral band
$l_2, l_3, l_4, \ldots, l_n$ = the l_2th, l_3th, l_4th, …, l_nth control volume
o = the oth sublayer, either sublayer $b-1$ or $b+1$
P_b = side of interface P_b facing toward the bth sublayer
$P_{b'}$ = side of interface P_b facing toward the $(b+1)$th sublayer
$t-t$ = refers to a infinite slab with two semitransparent surfaces
$1{-}b$ = a multilayer model composed of the layers from the first sublayer to the bth sublayer
$/\!/$, $\perp$ = components for parallel and perpendicular polarization, respectively

Superscripts

$a2_b$	=	surface, interface, or control volume of bth sublayer, used to define one-layer radiative intensity quotient transfer function
m	=	time step
n	=	the nth iterative calculation
nth	=	the nth-order scattering
P_b	=	side of interface P_b facing towards the bth sublayer
$P_{b'}$	=	side of interface P_b facing towards the $(b+1)$th sublayer
s	=	specular reflection
V_{J_b}	=	the Jth control volume in the bth sublayer
$*$	=	normalized values or dimensionless values

Introduction

COUPLED heat transfer of radiation and conduction in semitransparent materials has been of great interest over the past 40 years mainly because of its pervasive practical applications, such as ceramic components for high-temperature use, thermally protective coatings, glass forming for manufacturing, tempering of glass windows, porous burners and insulation systems, measurement for the thermal characterization of semitransparent materials, ceramic insulation for atmospheric reentry of spacecraft, and selected high-temperature components in advanced aircraft engines. In addition, researchers have examined coupled heat transfer in semitransparent media composed of single-layer,[1–3] two-layer,[4,5] three-layer,[6] and multilayered composites.[7–9] Because of additional mathematical and computational complexities, most of their research did not take into account transient effects of heat transfer. For combined heat transfer inside semitransparent materials, transient heat-transfer behavior must be analyzed, because translucence can cause internal temperature responses that are much more rapid and have distributions different from those due to heat conduction alone. Siegel[10] has given a detailed review of the transient effects of radiative heat transfer within semitransparent materials.

In a participating medium, heat transfer can be strongly affected by internal emission, absorption, reflection/refraction at semitransparent interfaces, and scattering of thermal radiation, because internal emission of radiation is proportional to the square of the refractive index, and reflection and refraction at a semitransparent interface are intimately related to the refractive index. At high temperature, a refractive index larger than 1 has a great effect on heat transfer. Siegel and Spuckler,[11,12] Spuckler and Siegel,[13] and Siegel[14,15] examined the influence of refractive index on radiative heat transfer[11,12,14,15] and combined heat transfer[13] in media with diffuse interfaces. Liu and Dougherty,[16] Crosbie and Shieh,[17] and Schwander et al.[18] analyzed Fresnel boundary reflection effects on heat transfer within media having a refractive index larger than unity. Considering refractive index to be a function of temperature and wavelength, Su and Sutton[19] solved a transient coupled heat-transfer problem in a nongray electromagnetic window with semitransparent specular surfaces. Siegel and Spuckler[20] studied the effects of refractive index and specular and diffuse reflection on radiative heat transfer in an isothermal layer with semitransparent surfaces. Luo et al.[9,21] considered the effect of refractive index on heat transfer in three-layer[21] and multilayered composites.[9]

Before 2000, all such research considered the refractive index to be constant within a medium or each sublayer of a composite medium. Radiative heat transfer inside a semitransparent medium with a continuously spatially varying refractive index (or graded index, GRIN) distribution has not been addressed until recent years. The pioneering work was done by Ben Abdallah and Le Dez,[22,23] who developed a curved ray-tracing technique for solving the radiative transfer problem within a graded index medium with black boundaries. After that, Lemonnier and Le Dez[24] used the discrete ordinates method; Huang et al.[25] and Xia et al.[26] adopted a curved ray-tracing method combined with a pseudo-source-adding method; Huang et al.[27] adopted a curved ray tracing method, and Liu[28] utilized a discrete curved ray-tracing method to examine the radiative transfer in a nonscattering medium with diffuse boundaries[24–26,28] and specular boundaries.[27] Liu et al.[29] utilized a discrete Monte Carlo curved ray-tracing method to investigate the radiative transfer in a nonscattering medium with diffuse boundaries. For scattering of radiant energy in a GRIN medium, the calculation is much more complicated. Ben Abdallah and coworkers[30,31] derived an integral form of the radiative transfer equation, with any spatially continuous refractive index and any phase function, from its integrodifferential form to solve the radiative transfer problem in an axisymmetric medium. Liu et al.[32] used a Monte Carlo curved ray-tracing method for radiative transfer in a scattering medium with a linear graded index and black boundaries and obtained temperature fields at radiative equilibrium. Huang et al.[33] proposed three different Monte Carlo ray-tracing strategies to study the radiative transfer in an absorbing–emitting–scattering slab with linear and sinusoidal refractive index distributions and specular surfaces and calculated thermal emission at radiative equilibrium. Reports of the coupled radiative and conductive heat transfer in a GRIN medium are much fewer than those of the heat transfer at radiative equilibrium as cited above. Ben Abdallah and Le Dez[23] investigated coupled radiation and conduction in a linearly varying refractive index slab with black surfaces by a curved ray-tracing method. Xia et al.[26] and Huang et al.[34] studied the same problem in a slab with diffuse boundaries using a curved ray-tracing technique in combination with a pseudo-source adding method[26] and semitransparent specular surfaces using a numerical curved ray-tracing method.[34] Liu and Tan[35] solved a transient coupled heat-transfer problem for a graded index slab with black surfaces analyzing the transient temperature response caused by pulsed irradiation. The above mentioned papers on coupled heat transfer in a GRIN medium did not consider scattering of radiant energy, and transient effects were considered in Ref. 35 only.

Luo et al.[9] and Tan et al.[36] developed a multilayer composite radiative transfer model using a ray-tracing method, combining node analysis and a spectral band model to solve for the transient heat transfer of coupled radiation and conduction within a scattering multilayer composite with specular interfaces. In each constant-refractive-index sublayer of the multilayered medium, a ray of radiation is a straight line. In a single-layer medium having a continuously varying refractive index, a ray travels in a curved continuous trajectory governed by the Fermat optical principle. In this paper, a single-layer slab with a graded refractive index is divided into a number of sublayers with a constant refractive index in each, and the radiative transfer in the GRIN slab is simulated by the multilayer transfer model. Both boundary surfaces of the single layer of a GRIN medium are semitransparent and specular, and the corresponding composite model is considered to be composed of semitransparent specular boundary surfaces and interfaces. In each sublayer, the refractive index is assumed to be constant, and the ray travels in a straight line instead of a curve. Errors caused by the assumption of constant refractive index in each sublayer, resulting in a straight-line radiative-transfer path instead of a curved path and specular reflection at each interface between two adjacent sublayers, will be reduced by increasing the number of layers. If the number of layers is big enough, the refractive index variation at each interface of each sublayer may be considered to be continuous, except for the case of possible total reflection at one interface. The specularly reflected part of the radiative energy should be negligible as compared to the refracted part, which would closely approach the actual radiative transfer inside a GRIN medium. By the same method used in Refs. 9 and 36, radiative transfer coefficients (RTCs) with scattering considered are deduced for a multilayered gray slab having semitransparent and specular boundary surfaces and interfaces, which helps to calculate the radiative heat source term. The transient energy equation for coupled radiative–conductive heat transfer is solved by a fully implicit control-volume method. Taking isotropic scattering of thermal radiation into account, transient thermal analysis is performed for a sinusoidally varying refractive index within a slab.

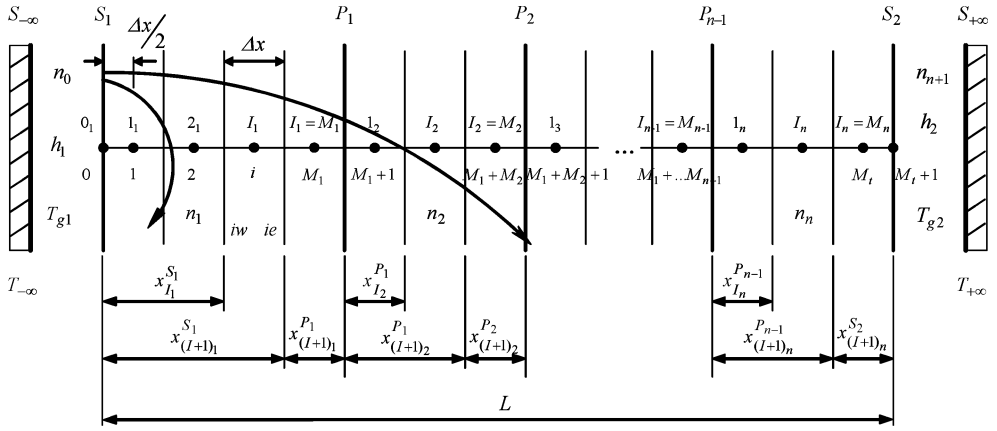

Fig. 1 Physical model of graded index medium discretized into *n* sublayers.

Analysis

Physical Model

As shown in Fig. 1, let us consider an absorbing–emitting–scattering gray infinite parallel plane slab of thickness L, having semitransparent specular surfaces S_1 and S_2 which are irradiated by two black surfaces $S_{-\infty}$ and $S_{+\infty}$ at temperatures of $T_{-\infty}$ and $T_{+\infty}$, respectively. Between S_1 and $S_{-\infty}$ and between $S_2$and $S_{+\infty}$ are gases whose temperatures are T_{g1} and T_{g2}, respectively. Thermal conductivity k, unit heat capacity C, extinction coefficient κ, and scattering albedo ω are assumed to be uniform, whereas refractive index is linearly or nonlinearly varying along slab thickness. To trace the radiative transfer within a GRIN medium, the medium can be divided into n sublayers. In each sublayer, refractive index is assumed to be constant, so that a ray of thermal radiation travels in a straight line instead of a curve. Interfaces between the two neighboring sublayers, such as $P_1, P_2, \ldots, P_{n-1}$ in Fig. 1, are semitransparent and specular, which reflect and refract thermal radiation by Fresnel's equation and Snell's law, respectively. Along slab thickness, the n sublayers are divided into $M_1, M_2, \ldots, M_n$ control volumes or interior nodes, respectively, where I_b is used to denote the Ith node in the bth sublayer. The total number of nodes is $M_t + 2 (0, 1, \ldots, M_t + 1)$, with node 0 located at S_1 and node $M_t + 1$ located at S_2. For convenience, all of the nodes are denoted by i as well, and if $b = 1$, $i = I_1$; otherwise if $1 < b \le n$, $i = (M_1 + M_2 + \cdots + M_{b-1}) + I_b$ (see Fig. 1).

Governing Equation

Transient coupled radiative–conductive heat transfer in a participating medium is governed by[5]

$$C\left(\frac{\partial T}{\partial t}\right) = -\mathrm{div}(q^{cd} + q^{r}) \tag{1}$$

According to Fig. 1, in a fully implicit form, the above energy equation is discretized into[5]

$$C\Delta x \frac{T_i^{m+1} - T_i^m}{\Delta t} = \frac{k_{ie}^{m+1}\left(T_{i+1}^{m+1} - T_i^{m+1}\right) - k_{iw}^{m+1}\left(T_i^{m+1} - T_{i-1}^{m+1}\right)}{\Delta x} + \Theta_i^{r,m+1} \tag{2}$$

In dimensionless form, Eq. (2) can be rewritten as

$$\frac{\Theta_i^{m+1} - \Theta_i^m}{\Delta t^*} = \frac{N_{ie}^{m+1}\left(\Theta_{i+1}^{m+1} - \Theta_i^{m+1}\right) - N_{iw}^{m+1}\left(\Theta_i^{m+1} - \Theta_{i-1}^{m+1}\right)}{\Delta X} + \Phi_i^{r^*,m+1} \tag{3}$$

where the dimensionless radiative heat source term of control volume i is equal to the difference between the dimensionless radiative heat flux densities at its two interfaces; that is, $\Phi_i^{r^*} = q_{iw}^{r^*} - q_{ie}^{r^*} = q_{(i-1)e}^{r^*} - q_{ie}^{r^*}$. By node analysis, the flux is[37]

$$q_{ie}^{r^*} = \frac{1}{4}\left\{ \sum_{j=1}^{i} \left([S_{+\infty}V_j]^s \Theta_{+\infty}^4 - n_j'^2 [V_j S_{+\infty}]^s \Theta_j^4\right) + \sum_{l=1}^{i} \sum_{j=i+1}^{M_t} \left(n_j'^2 [V_j V_l]^s \Theta_j^4 - n_l'^2 [V_l V_j]^s \Theta_l^4\right) + \sum_{j=i+1}^{M_t} \left(n_j'^2 [V_j S_{-\infty}]^s \Theta_j^4 - [S_{-\infty}V_j]^s \Theta_{-\infty}^4\right) + \left([S_{+\infty}S_{-\infty}]^s \Theta_{+\infty}^4 - [S_{-\infty}S_{+\infty}]^s \Theta_{-\infty}^4\right)\right\}$$

$$1 \le i, j \le M_t \tag{4}$$

where radiative transfer coefficients (RTCs), such as $[S_{+\infty}S_{-\infty}]^s$, $[S_{+\infty}V_j]^s$, and $[V_l V_j]^s$, are deduced by a ray-tracing method based on relations of energy transfer from surface to surface, surface to control volume, and control volume to control volume, using the zonal method.[38,39]

Consider a convection boundary condition as follows (taking S_1 as an example):

$$-k_1 \left.\frac{\partial T}{\partial x}\right|_{x=0} = h_1(T_{g1} - T_{S_1}) \tag{5}$$

Equation (5) can be also rewritten in discrete dimensionless form as[37]

$$8N_{1e}(\Theta_1 - \Theta_{S_1}) = H_1(\Theta_{S_1} - \Theta_{g1})\Delta X \tag{6}$$

Considering no convection at both boundaries, that is, $H_1 = H_2 = 0$, temperatures of the two boundary surfaces, T_{S1} and T_{S2}, equal the temperatures of interior node 1 and node M_t, that is, T_1 and T_{M_t}, respectively.

The key to solving the transient discrete energy equation [Eq. (2)] is to determine the local radiative heat source term ($\Phi_i^{r^*}$), and the difficulty in solving for that radiative heat source is in deducing the RTCs.

Radiative Transfer Coefficients for an *n*-Sublayer Slab

The RTC of element i (a surface or a control volume) with respect to element j is defined as quotient of the radiative energy absorbed by element j to the radiative energy emitted by element i. In a

scattering medium, depending upon the radiative transfer mechanism, the radiative transfer process can be classified into two subprocesses. The first one is an absorbing–emitting–reflecting subprocess, in which the radiative energy emitted by element i directly or indirectly [after being reflected by surfaces (or interfaces)] reaches element j, and such RTCs are denoted by $(S_{+\infty}S_{-\infty})^s$, $(S_{+\infty}V_j)^s$, $(V_iV_j)^s$, etc. The second is an absorbing–scattering subprocess, in which the radiative energy represented by the RTCs for the first subprocess is redistributed by scattering, and these RTCs are denoted by $[S_{+\infty}S_{-\infty}]^s$, $[S_{+\infty}V_j]^s$, $[V_iV_j]^s$, etc. Deduction of the RTCs for an n-sublayer slab starts with developing a multilayer radiative transfer model.

Multilayer Radiative Transfer Model for an Absorbing–Emitting Subprocess

To trace radiative transfer in a n-sublayer slab, multilayer radiative intensity quotient transfer functions are derived in this section. As shown in Fig. 2, for convenience in the following derivation, the notation for both sides of a semitransparent interface are specified as follows: $\overline{P_m}$ represents the interface between the mth and the $(m+1)$th layers, the side of the interface facing the mth layer is denoted as P_m, and the other side, facing the $(m+1)$th, layer is denoted as $P_{m'}$.

Single-layer radiative intensity quotient transfer functions, expressed by the symbol $\boldsymbol{F}_{a1_b}^{a2_b}$, are listed in Appendix B in Ref. 9. Multilayer radiative intensity quotient transfer functions are denoted by the symbol $\boldsymbol{H}_{b1,m+1\sim m+\Delta m}^{b2}$, which means the ratio of radiative intensity finally absorbed by interface $b2$ (represented by $P_{m'}$, $P_{m+1'}$, $P_{m+\Delta m-1}$ or $P_{m+\Delta m}$) to the radiative intensity emitted by interface $b1$ (represented by $P_{m'}$ or $P_{m+\Delta m}$) after that intensity has "transferred once" (defined as the process by which the radiative intensity is reflected and absorbed so many times that it finally becomes zero; see Ref. 20) inside a multilayer model (see Fig. 2). Subscript $m+1\sim m+\Delta m$ of the symbol $\boldsymbol{H}_{b1,m+1\sim m+\Delta m}^{b2}$ denotes that the multilayer model is composed of layers from the $(m+1)$th layer to the $(m+\Delta m)$th layer.

There are six kinds of multilayer radiative intensity quotient transfer functions:

$$\boldsymbol{H}_{P_{m'},m+1\sim m+\Delta m}^{P_{m'}},\quad \boldsymbol{H}_{P_{m'},m+1\sim m+\Delta m}^{P_{m+1'}},\quad H_{P_{m'},m+1\sim m+\Delta m}^{P_{m+\Delta m}}$$

$$H_{P_{m+\Delta m},m+1\sim m+\Delta m}^{P_{m+\Delta m}},\quad H_{P_{m+\Delta m},m+1\sim m+\Delta m}^{P_{m+\Delta m-1}}$$

$$H_{P_{m+\Delta m},m+1\sim m+\Delta m}^{P_{m'}}$$

The function

$$\boldsymbol{H}_{P_{m'},m+1\sim m+\Delta m}^{P_{m+\Delta m}},\quad \boldsymbol{H}_{P_{m'},m+1\sim m+\Delta m}^{P_{m+1'}},\quad \boldsymbol{H}_{P_{m'},m+1\sim m+\Delta m}^{P_{m'}}$$

are taken as examples to illustrate deduction of multilayer radiative intensity quotient transfer functions.

1) After the radiative intensity emitted by $P_{m'}$ "transfers once" within the $(m+\Delta m)$th layer, a fraction $F_{P_{m'}}^{P_{m+1}}\gamma(\theta)_{m+1,m+2}$ traverses $\overline{P_{m+1}}$ and enters the following $\Delta m-1$ layers. Then after "transferring once" within the $\Delta m-1$ layers, the fraction of radiative intensity reaching $P_{m+\Delta m}$ for the first time is

$$x_1 = \boldsymbol{F}_{P_{m'}}^{P_{m+1}}\gamma(\theta)_{m+1,m+2}\boldsymbol{H}_{P_{m+1'},m+2\sim m+\Delta m}^{P_{m+\Delta m}}$$

and that fraction reaching $P_{m+1'}$ for the first time is

$$y_1 = \boldsymbol{F}_{P_{m'}}^{P_{m+1}}\gamma(\theta)_{m+1,m+2}\boldsymbol{H}_{P_{m+1'},m+2\sim m+\Delta m}^{P_{m'+1}}$$

2) A fraction, $\gamma(\theta)_{m+2,m+1}$, of the radiative intensity that reaches $P_{m+1'}$ will enter the $(m+1)$th layer. Then after "transferring once" within the layer, a portion, $\gamma(\theta)_{m+2,m+1}F_{P_{m+1}}^{P_{m+1}}\gamma(\theta)_{m+1,m+2}$, will traverse $\overline{P_{m+1}}$ and enter the following $\Delta m-1$ layers. After "transferring once" within the $\Delta m-1$ layers, the fraction of radiative intensity emitted by $P_{m'}$ that reaches $P_{m+\Delta m}$ for the second time is

$$x_2 = y_1\gamma(\theta)_{m+2,m+1}\boldsymbol{F}_{P_{m+1}}^{P_{m+1}}\gamma(\theta)_{m+1,m+2}\boldsymbol{H}_{P_{m+1'},m+2\sim m+\Delta m}^{P_{m+\Delta m}}$$

and the fraction reaching $P_{m+1'}$ for the second time is

$$y_2 = y_1\gamma(\theta)_{m+2,m+1}\boldsymbol{F}_{P_{m+1}}^{P_{m+1}}\gamma(\theta)_{m+1,m+2}\boldsymbol{H}_{P_{m+1'},m+2\sim m+\Delta m}^{P_{m+1'}}$$

3) Repeating step 2 for quotient y_2, we can obtain the ratio of the radiative intensity emitted by $P_{m'}$ to that reaching $P_{m+\Delta m}$ for the third time,

$$x_3 = y_2\gamma(\theta)_{m+2,m+1}\boldsymbol{F}_{P_{m+1}}^{P_{m+1}}\gamma(\theta)_{m+1,m+2}\boldsymbol{H}_{P_{m+1'},m+2\sim m+\Delta m}^{P_{m+\Delta m}}$$

and the fraction reaching $P_{m+1'}$ for the third time is

$$y_3 = y_2\gamma(\theta)_{m+2,m+1}\boldsymbol{F}_{P_{m+1}}^{P_{m+1}}\gamma(\theta)_{m+1,m+2}\boldsymbol{H}_{P_{m+1'},m+2\sim m+\Delta m}^{P_{m+1'}}$$

In this way, the tracing process for quotient y_i can be repeated iteratively until it finally attenuates to zero. The total fraction of the radiative intensity, emitted by $P_{m'}$, which finally reaches $P_{m+\Delta m}$, can be calculated as follows:

$$\boldsymbol{H}_{P_{m'},m+1\sim m+\Delta m}^{P_{m+\Delta m}} = \sum_{i=1}^{\infty}x_i = x_1 + \frac{x_2}{1-\beta_2} \tag{7a}$$

where β_2 is a common ratio equal to

$$\gamma(\theta)_{m+2,m+1}\boldsymbol{F}_{P_{m+1}}^{P_{m+1}}\gamma(\theta)_{m+1,m+2}\boldsymbol{H}_{P_{m+1'},m+2\sim m+\Delta m}^{P_{m+1'}}$$

and $x_2, x_3\ldots$, is an infinite geometric progression with common ratio β_2. Radiative intensity gradually attenuates in a radiative transfer process, so $\beta_2<1$.

In a similar way, another multilayer radiative intensity quotient transfer function, $\boldsymbol{H}_{P_{m'},m+1\sim m+\Delta m}^{P_{m+1'}}$ can also be derived:

$$\boldsymbol{H}_{P_{m'},m+1\sim m+\Delta m}^{P_{m+1'}} = \sum_{i=1}^{\infty}y_i = \frac{y_1}{1-\beta_2} \tag{7b}$$

where $y_1, y_2, \ldots,$ is also an infinite geometric progression with common ratio β_2.

Using Eqs. (7a) and (7b), we can easily obtain the expression for $\boldsymbol{H}_{P_{m'},m+1\sim m+\Delta m}^{P_{m'}}$:

$$\boldsymbol{H}_{P_{m'},m+1\sim m+\Delta m}^{P_{m'}} = \boldsymbol{H}_{P_{m'},m+1\sim m+\Delta m}^{P_{m+1'}}\gamma(\theta)_{m+2,m+1}\boldsymbol{F}_{P_{m+1}}^{P_{m'}} \tag{7c}$$

Obviously, Eqs. (7a–7c) are a group of recursive formulas, and their calculation should be started from the $(m+\Delta m)$th layer at first; that is,

$$\boldsymbol{H}_{P_{m+\Delta m-1'},m+\Delta m\sim m+\Delta m}^{P_{m+\Delta m-1'}} = \boldsymbol{F}_{P_{m+\Delta m-1'}}^{P_{m+\Delta m-1'}}$$

$$\boldsymbol{H}_{P_{m+\Delta m-1'},m+\Delta m\sim m+\Delta m}^{P_{m+\Delta m}} = \boldsymbol{F}_{P_{m+\Delta m-1'}}^{P_{m+\Delta m}}$$

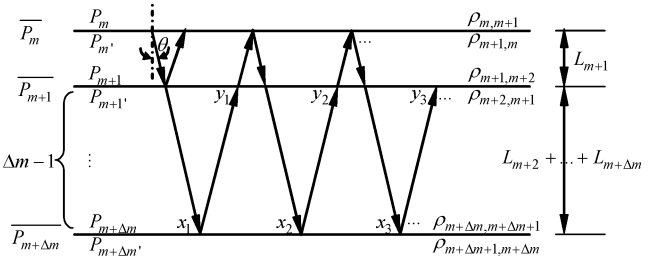

Fig. 2 Multilayer radiative transfer model.

Based on these two equations and combined with one-layer radiative intensity quotient transfer functions of the layer $(m+\Delta m-1)$, quotients

$$\boldsymbol{H}^{P_{m+\Delta m-1'}}_{P_{m+\Delta m-2'},m+\Delta m-1\sim m+\Delta m}, \qquad \boldsymbol{H}^{P_{m+\Delta m-2'}}_{P_{m+\Delta m-2'},m+\Delta m-1\sim m+\Delta m}$$

$$\boldsymbol{H}^{P_{m+\Delta m}}_{P_{m+\Delta m-2'},m+\Delta m-1\sim m+\Delta m}$$

can be calculated from Eqs. (7). Similarly, based on

$$\boldsymbol{H}^{P_{m+\Delta m-2'}}_{P_{m+\Delta m-2'},m+\Delta m-1\sim m+\Delta m}, \qquad \boldsymbol{H}^{P_{m+\Delta m}}_{P_{m+\Delta m-2'},m+\Delta m-1\sim m+\Delta m}$$

and combining one-layer radiative intensity quotient transfer functions of the layer $(m+\Delta m-2)$,

$$\boldsymbol{H}^{P_{m+\Delta m-2'}}_{P_{m+\Delta m-3'},m+\Delta m-2\sim m+\Delta m}, \qquad \boldsymbol{H}^{P_{m+\Delta m-3'}}_{P_{m+\Delta m-3'},m+\Delta m-2\sim m+\Delta m}$$

$$\boldsymbol{H}^{P_{m+\Delta m}}_{P_{m+\Delta m-3'},m+\Delta m-2\sim m+\Delta m}$$

can be calculated from Eqs. (7). Therefore, repeating the calculations in such a way, quotients

$$\boldsymbol{H}^{P_{m+\Delta m}}_{P_{m'},m+1\sim m+\Delta m}, \qquad \boldsymbol{H}^{P_{m+1'}}_{P_{m'},m+1\sim m+\Delta m}$$

$$\boldsymbol{H}^{P_{m'}}_{P_{m'},m+1\sim m+\Delta m}$$

can finally be calculated. The expressions $\rho(\theta)$ and $\gamma(\theta)$ in Eqs. (5) are functions of polarized components, as shown in Appendix A of Ref. 9.

Similarly, we can also obtain expressions for

$$\boldsymbol{H}^{P_{m+\Delta m}}_{P_{m+\Delta m},m+1\sim m+\Delta m}, \qquad \boldsymbol{H}^{P_{m+\Delta m-1}}_{P_{m+\Delta m},m+1\sim m+\Delta m}$$

$$\boldsymbol{H}^{P_{m'}}_{P_{m+\Delta m},m+1\sim m+\Delta m}$$

or one can get detailed information on derivations of the above three multilayer radiative intensity quotient transfer functions from our previous paper.[9]

Radiative Transfer Coefficients of an n-Sublayer Slab for Absorbing–Emitting Subprocess

With the aid of the multilayer radiative intensity quotient transfer functions deduced in the previous section and the single-layer radiative intensity quotient transfer functions presented of Appendix B in Ref. 9, RTCs of an n-sublayer slab for an absorbing–emitting subprocess can be calculated. Now we take $(V_{I_a}V_{J_b})^s_{t-t}$ as an example to illustrate the deduction of RTCs.

The process for tracing the transfer of the radiative intensity emitted by control volume V_{I_a} in an n-sublayer slab takes two steps to complete. In the upper tracing process shown in Fig. 3a, after the radiative intensity emitted by V_{I_a} transfers once in upper sublayers from layer 1 to layer $b-1$, the fraction of radiative intensity reaching P_{b-1} is deduced first. Then, in the process shown in Fig. 3b, the radiative transfer is traced in an n-sublayer medium, the total fraction reaching P_{b-1} and $P_{b'}$ can be calculated, and finally the expression for $(V_{I_a}V_{J_b})^s_{t-t}$ can be obtained.

1) *Step one*. As shown in Fig. 3a, the radiative intensity emitted by V_{I_a} transfers in two directions. After the intensity transfers once in sublayer a, one part, $w'_1=\boldsymbol{F}^{P_{a-1'}}_{V_{I_a}}$, will reach $P_{a-1'}$, and the other part, $x'_1=\boldsymbol{F}^{P_a}_{V_{I_a}}$, will reach P_a. To calculate the fraction of the radiative intensity emitted by V_{I_a} that reaches P_{b-1}, the two-part transfer is traced in the previous $b-1$ sublayers as follows.

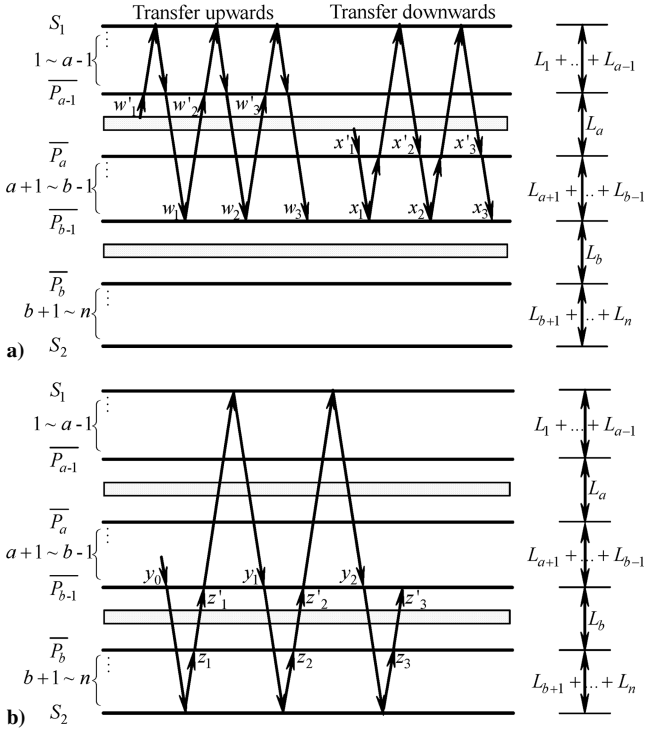

Fig. 3 Ray trajectories of RTC $(V_{I_a}V_{J_b})^s_{t-t}$.

A fraction, w'_1, transfers upwards. A part, $\gamma(\theta)_{a,a-1}$, of that fraction penetrates $\overline{P_{a-1}}$ and enters the previous $a-1$ sublayers. After it transfers once, the fraction $w'_1\gamma(\theta)_{a,a-1}\boldsymbol{H}^{P_{a-1}}_{P_{a-1},1\sim a-1}$ reaches P_{a-1}, and a part, $\gamma(\theta)_{a-1,a}$, of that fraction penetrates $\overline{P_{a-1}}$ and enters the following layers, $a-b-1$, and after transferring once therein, the fraction reaching P_{b-1} for the first time is

$$w_1=w'_1\gamma(\theta)_{a,a-1}\boldsymbol{H}^{P_{a-1}}_{P_{a-1},1\sim a-1}\gamma(\theta)_{a-1,a}\boldsymbol{H}^{P_{b-1}}_{P_{a-1'},a\sim b-1}$$

and the fraction

$$w'_2=w'_1\gamma(\theta)_{a,a-1}\boldsymbol{H}^{P_{a-1}}_{P_{a-1},1\sim a-1}\gamma(\theta)_{a-1,a}\boldsymbol{H}^{P_{a-1'}}_{P_{a-1'},a\sim b-1}$$

reaches $P_{a-1'}$. The fraction w'_2 repeats this transfer process, and the fraction reaching P_{b-1} for the second time is

$$w_2=w'_2\gamma(\theta)_{a,a-1}\boldsymbol{H}^{P_{a-1}}_{P_{a-1},1\sim a-1}\gamma(\theta)_{a-1,a}\boldsymbol{H}^{P_{b-1}}_{P_{a-1'},a\sim b-1}$$

whereas the fraction

$$w'_3=w'_2\gamma(\theta)_{a,a-1}\boldsymbol{H}^{P_{a-1}}_{P_{a-1},1\sim a-1}\gamma(\theta)_{a-1,a}\boldsymbol{H}^{P_{a-1'}}_{P_{a-1'},a\sim b-1}$$

reaches $P_{a-1'}$.

The tracing process for the fraction w_i can be repeated iteratively, until it finally attenuates to zero, and the fraction of radiative intensity emitted upward by V_{I_a} and finally reaching P_{b-1} can be calculated as follows:

$$w=\sum_{i=1}^{\infty}w_i$$

$$=\frac{\boldsymbol{F}^{P_{a-1'}}_{V_{I_a}}\gamma(\theta)_{a,a-1}\boldsymbol{H}^{P_{a-1}}_{P_{a-1},1\sim a-1}\gamma(\theta)_{a-1,a}\boldsymbol{H}^{P_{b-1}}_{P_{a-1'},a\sim b-1}}{1-\beta_3} \tag{8a}$$

where $\beta_3=\gamma(\theta)_{a,a-1}\boldsymbol{H}^{P_{a-1}}_{P_{a-1},1\sim a-1}\gamma(\theta)_{a-1,a}\boldsymbol{H}^{P_{a-1'}}_{P_{a-1'},a\sim b-1}$. If $a=1$, then $w=0$.

In a similar way, tracing the radiative transfer of part x'_1 in the sublayers $1-b-1$, we can calculate the fraction of radiative intensity emitted downward by V_{I_a} finally reaching P_{b-1} as follows:

$$x=\sum_{i=1}^{\infty}x_i=\frac{\boldsymbol{F}^{P_a}_{V_{I_a}}\gamma(\theta)_{a,a+1}\boldsymbol{H}^{P_{b-1}}_{P_{a'},a+1\sim b-1}}{1-\beta_4} \tag{8b}$$

where

$$\beta_4 = \gamma(\theta)_{a,a+1}\boldsymbol{H}^{P_{a'}}_{P_{a'},a+1\sim b-1}\gamma(\theta)_{a+1,a}\boldsymbol{H}^{P_a}_{P_a,1\sim a}$$

If $a = b-1$, then $x = \boldsymbol{F}^{P_a}_{V_{I_a}}$.

Therefore, the total fraction of the radiative intensity emitted in both directions by V_{I_a} that finally reaches P_{b-1} for the first time is

$$y_0 = w + x \tag{9}$$

2) *Step two*. As shown in Fig. 3b, a fraction, $\gamma(\theta)_{b-1,b}$, of the y_0 portion penetrates $\overline{P_{b-1}}$ and enters the following $b\sim n$ sublayers. After it "transfers once" therein, the fraction reaching $P_{b'}$ for the first time is

$$z_1 = y_0\gamma(\theta)_{b-1,b}\boldsymbol{H}^{P_{b'}}_{P_{b-1'},b\sim n}$$

and that fraction reaching $P_{b-1'}$ for the first time is

$$z_1' = y_0\gamma(\theta)_{b-1,b}\boldsymbol{H}^{P_{b-1'}}_{P_{b-1'},b\sim n}$$

A fraction $\gamma(\theta)_{b,b-1}$ of z_1' penetrates $\overline{P_{b-1}}$ and enters previous sublayers $1-b-1$. After it transfers once therein, the fraction reaching P_{b-1} for the first time is

$$y_1 = z_1'\gamma(\theta)_{b,b-1}\boldsymbol{H}^{P_{b-1}}_{P_{b-1},1\sim b-1}$$

The fraction y_1 repeats the above transfer process of y_0 and the fraction reaching $P_{b'}$ for the second time is

$$z_2 = y_1\gamma(\theta)_{b-1,b}\boldsymbol{H}^{P_{b'}}_{P_{b-1'},b\sim n}$$

and that fraction reaching $P_{b-1'}$ for the second time is

$$z_2' = y_1\gamma(\theta)_{b-1,b}\boldsymbol{H}^{P_{b-1'}}_{P_{b-1'},b\sim n}$$

z_2' repeats the above transfer process of z_1', and the fraction reaching P_{b-1} for the second time is

$$y_2 = z_2'\gamma(\theta)_{b,b-1}\boldsymbol{H}^{P_{b-1}}_{P_{b-1},1\sim b-1}$$

The tracing process for y_i and z_i can be repeated iteratively, until they finally attenuate to zero. The fractions of the radiative intensity emitted by V_{I_a} that finally reaches P_{b-1} and $P_{b'}$ are

$$y = \sum_{i=0}^{\infty} y_i = \frac{y_0}{1-\beta_5} \tag{10}$$

and

$$z = \sum_{i=0}^{\infty} z_i = \frac{z_1}{1-\beta_5} \tag{11}$$

respectively, with

$$\beta_5 = \gamma(\theta)_{b-1,b}\boldsymbol{H}^{P_{b-1'}}_{P_{b-1'},b\sim n}\gamma(\theta)_{b,b-1}\boldsymbol{H}^{P_{b-1}}_{P_{b-1},1\sim b-1}$$

A portion, $\gamma(\theta)_{b-1,b}$, of y and a portion, $\gamma(\theta)_{b+1,b}$, of z enter the bth sublayer and transfer once therein. Thus, the total fraction of the radiative intensity emitted by V_{I_a} that is finally absorbed by control-volume V_{J_b} can be obtained as follows:

$$\Gamma(\theta) = y\gamma(\theta)_{b-1,b}\boldsymbol{F}^{V_{J_b}}_{P_{b-1'}} + z\gamma(\theta)_{b+1,b}\boldsymbol{F}^{V_{J_b}}_{P_b} \tag{12}$$

which is suitable for $b \neq n$. If $b = n$, then $z = 0$.

Note that $\Gamma(\theta)$ is a function of polarized components, and for unpolarized incident radiative intensity, the total fraction absorbed by V_{J_b} can be expressed as

$$f(\theta) = [\Gamma_{/\!/}(\theta) + \Gamma_{\perp}(\theta)]/2 \tag{13}$$

Integrating $f(\theta)$ over all hemispherical directions can give $(V_{I_a}V_{J_b})^s_{t-t}$. The function $f(\theta)$ cannot be integrated directly, because it is a discontinuous function over the hemisphere because of total reflection. For this reason, we adopt the following technique to make $f(\theta)$ continuous[9]:

1) Critical angles of the bth sublayer with other sublayers and with surroundings for total reflection to occur are solved. If $n_b > n_a (a = 0\sim n+1)$, $\theta'_{ba} = \arcsin(n_a/n_b)$. Otherwise, if $n_b \le n_a$, no total reflection can occur, and therefore $\theta'_{ba} = \pi/2$. Then, $n+2$ critical angles, $\theta'_{b0}, \theta'_{b1}, \theta'_{b2}, \ldots, \theta'_{bn}$, and $\theta'_{b(n+1)}$, can be obtained, where θ'_{bb} must be equal to the biggest angle, $\pi/2$.

2) Rearrange these angles from the smallest to the largest, and assumes the order to be $\theta_{b(-1)}(=0) < \theta_{b0} \le \theta_{b1} \le \theta_{b2} \le \cdots \le \theta_{b(n+1)}(=\pi/2)$.

This means that all the hemispherical directions are divided into $n+2$ intervals separated by those critical angles, that is, $[\theta_{b(-1)}, \theta_{b0}], [\theta_{b0}, \theta_{b1}], \ldots, [\theta_{bn}, \theta_{b(n+1)}]$, and, within each interval, the function $f(\theta)$ can become continuous. Thus,

$$(V_{I_a}V_{J_b})^s_{t-t} = 2\sum_{i=-1}^{n}\int_{\theta_{bi}}^{\theta_{b(i+1)}} f(\theta)\cos\theta\,\sin\theta\,\mathrm{d}\theta \tag{14}$$

What needs to be emphasized in Eq. (14) is that the criterion for total reflection to occur, as discussed in Appendix A in Ref. 9, must be used when this equation is integrated. In this way, other RTCs can be determined as well.

Radiative Transfer Coefficients of an *n*-Sublayer Slab for Absorbing–Scattering Subprocess

In considering scattering effects, quotients of the radiative intensity represented by RTCs such as $(S_{+\infty}S_{-\infty})^s_{t-t}$, $(S_{+\infty}V_j)^s_{t-t}$, $(V_jV_l)^s_{t-t}$ will be redistributed by scattering. Before that, RTCs for an absorbing–emitting subprocess must be normalized as follows:

$$(V_iV_j)^{s^*}_{t-t} = (V_iV_j)^s_{t-t}/(4\kappa_b\Delta x_b) \qquad V_i \in b\text{th sublayer} \tag{15a}$$

$$(V_iS_u)^{s^*}_{t-t} = (V_iS_u)^s_{t-t}/(4\kappa_b\Delta x_b) \qquad V_i \in b\text{th sublayer} \tag{15b}$$

$$(S_uV_j)^{s^*}_{t-t} = (S_uV_j)^s_{t-t} \tag{15c}$$

$$(S_uS_v)^{s^*}_{t-t} = (S_uS_v)^s_{t-t} \tag{15d}$$

The process of deducing RTCs, when isotropic scattering is considered, is given by $[V_{I_a}V_{J_b}]^s_{t-t}$ as an example. For convenience, subscript $t-t$ and superscript s are omitted. Subscript a is introduced to denote the absorption fraction. Notice that it is only applied to a medium that scatters radiation, not to surfaces.

1) After the first-order scattering, in the quotient of the radiative energy denoted by RTC (V_iV_j), only a portion η_j is absorbed; that is, $[V_iV_j]^{*1\mathrm{st}}_a = (V_iV_j)^*\eta_j$.

2) After the second-order scattering, the fraction of the energy emitted by V_i, scattered by all control volumes, is $(V_iV_{l_2})^*\omega'_{l_2}$, which is distributed uniformly in a medium and equivalent to that isotropically emitted by control volumes. In the fraction, a portion η_j of the $(V_{l_2}V_j)^*$ reaching V_j is absorbed; that is,

$$[V_iV_j]^{*2\mathrm{nd}}_a = [V_iV_j]^{*1\mathrm{st}}_a + \sum_{l_2=1}^{M_t}(V_iV_{l_2})^*\omega'_{l_2}(V_{l_2}V_j)^*\eta_j$$

3) After the third-order scattering, a similar analysis leads to

$$[V_iV_j]^{*3\mathrm{rd}}_a = [V_iV_j]^{*2\mathrm{nd}}_a + \sum_{l_2=1}^{M_t}(V_iV_{l_2})^*\omega'_{l_2}\left[\sum_{l_3=1}^{M_t}(V_{l_2}V_{l_3})^*\omega'_{l_3}(V_{l_3}V_j)^*\eta_j\right]$$

4) Trace the scattered energy repeatedly as shown. After the nth-order scattering, if the criteria

$$\left|1-[V_iV_j]_a^{*n\text{th}}\right|<10^{-10}$$

can be satisfied by all control volumes, the calculation is finished. Thus,

$$[V_iV_j]_a^{*n\text{th}}=[V_iV_j]_a^{*(n-1)\text{th}}+\sum_{l_2=1}^{M_t}\left(V_iV_{l_2}\right)^*\omega'_{l_2}\left\{\sum_{l_3=1}^{M_t}\left(V_{l_2}V_{l_3}\right)^*\omega'_{l_3}\left\{\sum_{l_4=1}^{M_t}\left(V_{l_3}V_{l_4}\right)^*\omega'_{l_4}\cdots\left\{\sum_{l_{n-1}=1}^{M_t}\left(V_{l_{n-2}}V_{l_{n-1}}\right)^*\omega'_{l_{n-1}}\times\left[\sum_{l_n=1}^{M_t}\left(V_{l_{n-1}}V_{l_n}\right)^*\omega'_{l_n}(V_iV_j)^*\eta_j\right]\right\}\right\}\right\} \tag{16a}$$

Finally, through inverse calculation and considering the emissive power of control volumes, $[V_iV_j]$ can be obtained: $[V_iV_j]=4\kappa_b\eta_b\Delta x_b[V_iV_j]_a^{*n\text{th}}$, where $V_i\in b$th sublayer. Similarly, after the nth-order scattering, $[S_uS_v]=[S_uS_v]_a^{*n\text{th}}$, $[S_uV_j]=[S_uV_j]_a^{*n\text{th}}$, and $[V_iS_u]=4\kappa_b\eta_b\Delta x_b[V_iS_u]_a^{*n\text{th}}$ can be determined, where

$$[S_uS_v]_a^{*n\text{th}}=[S_uS_v]_a^{*(n-1)\text{th}}+\sum_{l_2=1}^{M_t}\left(S_uV_{l_2}\right)^*\omega'_{l_2}\left\{\sum_{l_3=1}^{M_t}\left(V_{l_2}V_{l_3}\right)^*\omega'_{l_3}\left\{\sum_{l_4=1}^{M_t}\left(V_{l_3}V_{l_4}\right)^*\omega'_{l_4}\cdots\left\{\sum_{l_{n-1}=1}^{M_t}\left(V_{l_{n-2}}V_{l_{n-1}}\right)^*\omega'_{l_{n-1}}\times\left[\sum_{l_n=1}^{M_t}\left(V_{l_{n-1}}V_{l_n}\right)^*\omega'_{l_n}\left(V_{l_n}S_v\right)^*\right]\right\}\right\}\right\} \tag{16b}$$

$$[V_iS_u]_a^{*n\text{th}}=[V_iS_u]_a^{*(n-1)\text{th}}+\sum_{l_2=1}^{M_t}\left(V_iV_{l_2}\right)^*\omega'_{l_2}\left\{\sum_{l_3=1}^{M_t}\left(V_{l_2}V_{l_3}\right)^*\omega'_{l_3}\left\{\sum_{l_4=1}^{M_t}\left(V_{l_3}V_{l_4}\right)^*\omega'_{l_4}\cdots\left\{\sum_{l_{n-1}=1}^{M_t}\left(V_{l_{n-2}}V_{l_{n-1}}\right)^*\omega'_{l_{n-1}}\times\left[\sum_{l_n=1}^{M_t}\left(V_{l_{n-1}}V_{l_n}\right)^*\omega'_{l_n}\left(V_{l_n}S_u\right)^*\right]\right\}\right\}\right\} \tag{16c}$$

$$[S_uV_j]_a^{*n\text{th}}=[S_uV_j]_a^{*(n-1)\text{th}}+\sum_{l_2=1}^{M_t}\left(S_uV_{l_2}\right)^*\omega'_{l_2}\left\{\sum_{l_3=1}^{M_t}\left(V_{l_2}V_{l_3}\right)^*\omega'_{l_3}\left\{\sum_{l_4=1}^{M_t}\left(V_{l_3}V_{l_4}\right)^*\omega'_{l_4}\cdots\left\{\sum_{l_{n-1}=1}^{M_t}\left(V_{l_{n-2}}V_{l_{n-1}}\right)^*\omega'_{l_{n-1}}\times\left[\sum_{l_n=1}^{M_t}\left(V_{l_{n-1}}V_{l_n}\right)^*\omega'_{l_n}\left(V_{l_n}V_j\right)^*\eta_j\right]\right\}\right\}\right\} \tag{16d}$$

Numerical Method and Validations for Radiative Transfer Coefficients

Numerical Method

Dimensionless radiative heat source term $\Phi_i^{r^*}$ is a nonlinear function of dimensionless temperature Θ_i, so it must be treated first with linearization by Patankar's method:

$$\begin{aligned}\Phi_i^{r^*,m,n+1}&=\Phi_i^{r^*,m,n}+\left(d\Phi_i^{r^*}\big/d\Theta_i\right)^{m,n}\left(\Theta_i^{m,n+1}-\Theta_i^{m,n}\right)\\&=Sc_i^{m,n+1}+Sp_i{}^{m,n+1}\Theta_i^{m,n+1}\end{aligned} \tag{17}$$

where superscripts n and $n+1$ denote the nth and $(n+1)$th iterative calculations; Sc_i represents the constant part of $\Phi_i^{r^*}$; Sp_i is the modulus of Θ_i, and $Sp_i\le 0$. After linearization of the nonlinear term in Eq. (2) or Eq. (3), a group of linear equations can be obtained that could be solved by TDMA (tridiagonal matrix algorithm), and consequently, temperatures of all nodes can be evaluated.

Validations for Radiative Transfer Coefficients

For RTCs of the absorbing–emitting subprocess, the following reciprocal relationships must be satisfied:

$$n_a^2\left(V_{I_a}V_{J_b}\right)_{t-t}^s=n_b^2\left(V_{J_b}V_{I_a}\right)_{t-t}^s \tag{18a}$$

$$n_a^2\left(V_{I_a}S_{+\infty}\right)_{t-t}^s=\left(S_{+\infty}V_{I_a}\right)_{t-t}^s \tag{18b}$$

$$\left(S_{-\infty}V_{I_b}\right)_{t-t}^s=n_b^2\left(V_{I_b}S_{-\infty}\right)_{t-t}^s \tag{18c}$$

$$(S_{-\infty}S_{+\infty})_{t-t}^s=(S_{+\infty}S_{-\infty})_{t-t}^s \tag{18d}$$

For RTCs of the absorbing-scattering subprocess, the relationships of integrality must be satisfied as below:

$$\sum_{j=1}^{M_t}[V_iV_j]_{k,t-t}^s+[V_iS_{-\infty}]_{k,t-t}^s+[V_iS_{+\infty}]_{k,t-t}^s=4\kappa_b\eta_b\Delta x_b \tag{19a}$$

$$[S_{-\infty}S_{-\infty}]_{k,t-t}^s+\sum_{j=1}^{M_t}[S_{-\infty}V_j]_{k,t-t}^s+[S_{-\infty}S_{+\infty}]_{k,t-t}^s=1 \tag{19b}$$

$$[S_{+\infty}S_{-\infty}]_{k,t-t}^s+\sum_{j=1}^{M_t}[S_{+\infty}V_j]_{k,t-t}^s+[S_{+\infty}S_{-\infty}]_{k,t-t}^s=1 \tag{19c}$$

Using a 30-point improved Gaussian quadrature scheme, expressions for RTC as Eq. (14) are numerically calculated. Choose 10^{-9} as the precision of Gaussian quadrature scheme. With this precision, errors for the satisfaction of Eqs. (18) and (19) are smaller than 10^{-10}, which shows that Eqs. (18) and (19) are satisfied very well.

Results and Analysis

To simulate the radiative transfer inside a GRIN slab using the multilayer model of specular reflection developed above, discrete sublayer number n should be large enough, and in each sublayer, the number of control volumes must be equal to unity, that is, $M_1=M_2=\cdots=M_n=1$. In addition, assume $\kappa=\kappa_1=\kappa_2=\cdots=\kappa_n$, $\omega=\omega_1=\omega_2=\cdots\omega_n$ and $k=k_1=k_2=\cdots k_n$ in the current multilayer model.

Comparison with Reference 34

Reference 34 examined combined radiative and conductive heat transfer within an absorbing–emitting slab of semitransparent gray medium with semitransparent specular boundaries at steady state. Linear and nonlinear graded refractive index distributions were considered in Ref. 34. Figure 4a provides a comparison of present results with Ref. 34 for $n(X)=1.2+0.6X$,

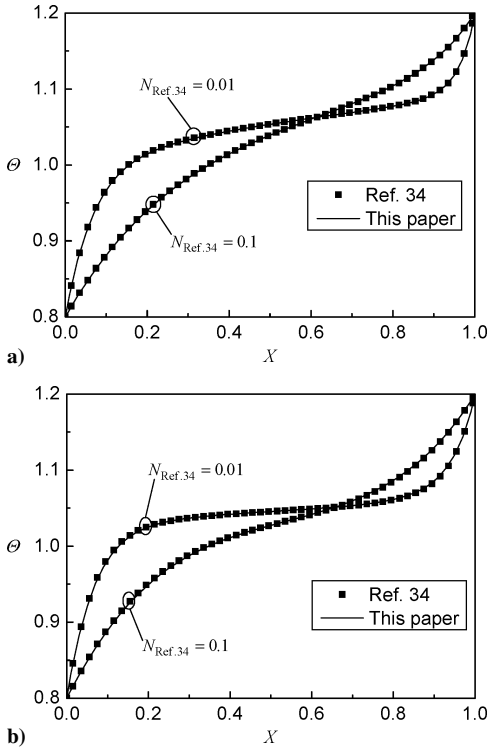

Fig. 4 Comparison of temperature distributions with Ref. 34 at radiative conductive coupling: a) $n(X) = 1.2 + 0.6X$, b) $n(X) = 1.2 + 0.6\sin(\pi X)$.

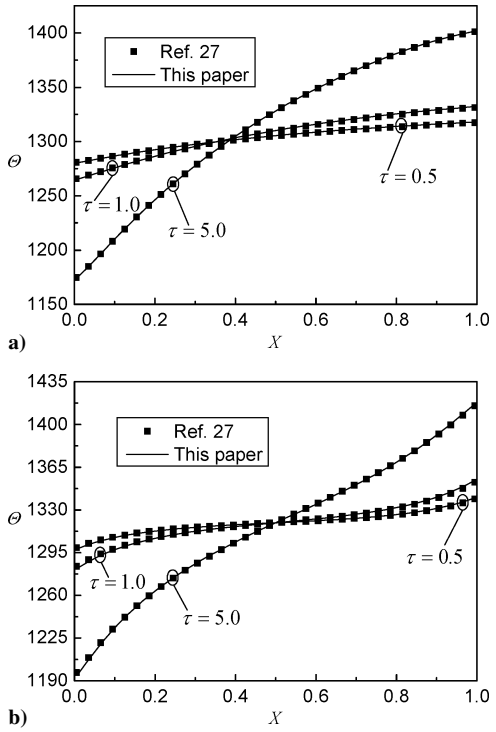

Fig. 5 Comparison of temperature distributions with Ref. 27 at radiative equilibrium: a) $n(X) = 1.2 + 0.6X$, b) $n(X) = 1.2 + 0.6\sin(\pi X)$.

and Fig. 4b is for $n(X) = 1.2 + 0.6\sin(\pi X)$. The solid lines are results of this paper, and the square symbols denote results of Ref. 34. In this paper, for comparison, parameters are assumed to be $n = 50$, $H_1 = H_2 = \infty$, $\tau = 1$, $\omega = 0$, $\Theta_{-\infty} = \Theta_{g1} = 0.8$, and $\Theta_{+\infty} = \Theta_{g2} = 1.2$. According to Ref. 34, a conduction–radiation parameter is defined as $N_{\text{Ref. }34} = k\kappa/4\sigma n_R^2 T_R^3$, where n_R is a reference refractive index, specified as 1.5; T_R is a reference temperature, equal to $(T_{+\infty} + T_{-\infty})/2$. As shown in Fig. 4, results of this paper are almost the same as those of Ref. 34, which demonstrates that the multilayer model of specular reflection used to simulate the radiative heat transfer coupled with conduction inside a nonscattering GRIN slab is rational and correct.

Comparison with Ref. 27

Reference 27 investigated temperature fields in participating nonscattering media having linear and nonlinear graded refractive indexes at radiative equilibrium. The medium boundaries were semitransparent and specular. Results of this paper comparing with Ref. 27 for $n(X) = 1.2 + 0.6X$ and $n(X) = 1.2 + 0.6\sin(\pi X)$ are plotted in Figs. 5a and 5b. The solid lines are results of this paper, and the square symbols denote results of Ref. 27. In this paper, for comparison, parameters are taken as $n = 50$, $H_1 = H_2 = 0$, $N_{ie} = N_{iw} = 0$, $\omega = 0$, $T_{-\infty} = 1000$ K, and $T_{+\infty} = 1500$ K. From Fig. 5, we can see that for different refractive index distributions and different optical thickness, temperature profiles calculated by the multilayer model of radiative transfer developed in this paper accord very well with those by the curved ray-tracing method in Ref. 27. This proves again that the multilayer simulation of radiative transfer in a graded refractive index medium is correct and reliable.

Transient Coupled Radiation and Conduction in a Nonlinear Graded Refractive Index Slab

Using the multilayer model of specular reflection developed here to simulate radiative transfer inside a GRIN medium, transient temperature distributions for radiative conductive coupling in a nonlinear graded refractive index scattering slab having specular semitransparent surfaces is investigated, mainly discussing effects of scattering albedo and optical thickness on temperature peaks in the slab.

It is pointed out in Ref. 40 that for combined heat transfer by radiation and conduction, a temperature peak will appear in a medium with homogeneous properties if the following four conditions are satisfied simultaneously: 1) the medium being semitransparent; 2) the boundary surfaces being semitransparent; 3) the surfaces being subjected to external radiation; 4) the heated surface being cooled by surrounding convection. It is discovered in Ref. 6 that for an inhomogeneous medium, even though its surfaces are not cooled by convection, if the absorption coefficient (or extinction coefficient) of inner regions is higher than that of outer regions, a temperature peak will appear because inner regions will absorb more radiative energy. Further analyzing, under no convection at both semitransparent boundaries, if a refractive index gradient exists through a slab, can a temperature peak appears even though absorption coefficient (or extinction coefficient) is supposed to be uniform? Up to now, research on this problem has not been found.

Common parameters for the calculations are $n = 50$, $C = 10^5$ J m^{-3} K^{-1}, $H_1 = H_2 = 0$, $N_{ie} = N_{iw} = 0.005$, $L = 0.01$ m, $T_r = 1000$ K, $\Theta_0 = 0.75$, $\Theta_\infty = 3$, and $\Theta_{+\infty} = 1$. Sinusoidal distribution of a refractive index is assumed and

$$n(X) = n_s + (n_c - n_s)\sin(\pi X) \tag{20}$$

where n_s is a refractive index value at surfaces and n_c is that at the center position of the slab, and the sum of n_s and n_c is kept unchanged and equal to 4 in Figs. 6–9. Because thermal emission within a slab is proportional to n^2, under the same conditions, for $n_s > n_c$, emissive power in outer regions is stronger than that in inner regions; and for $n_s < n_c$, emissive power in inner regions is stronger than that in outer regions.

Figure 6 considers the case of $\omega = 0$ and shows effects of different optical thickness on transient temperature fields in a GRIN slab. From Fig. 6, we can see that temperature peaks exist in center region of the slab without convection at both boundaries when the absorption coefficient is spatially uniform. For an optically thin medium with $\tau = 0.05$, as in Fig. 6a, temperature profiles in outer region are flat because of weak absorption of the radiative energy; while in inner region, for $n_c < n_s$, weaker emissive power therein cause inner regions to release less energy and absorb more from external black surroundings, which to a large extent results in appearance of temperature peaks, and, with increasing of a refractive index gradient,

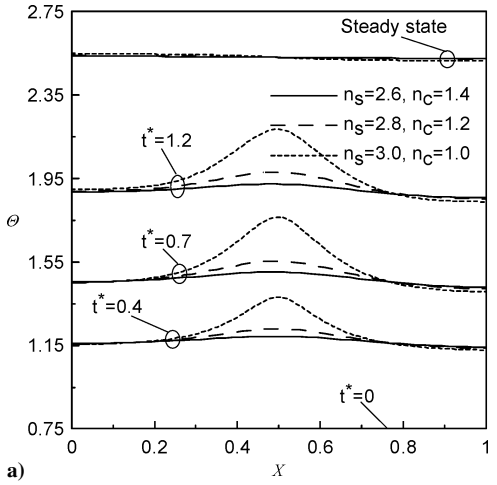

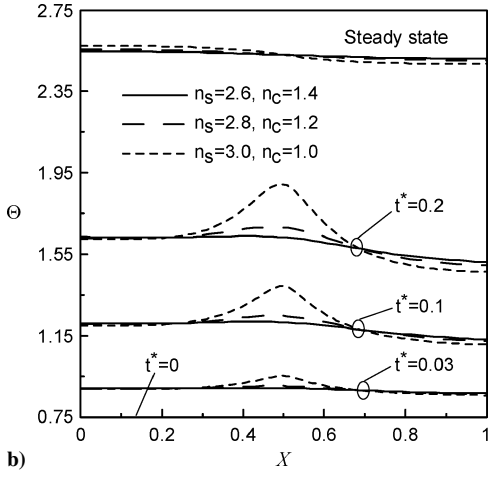

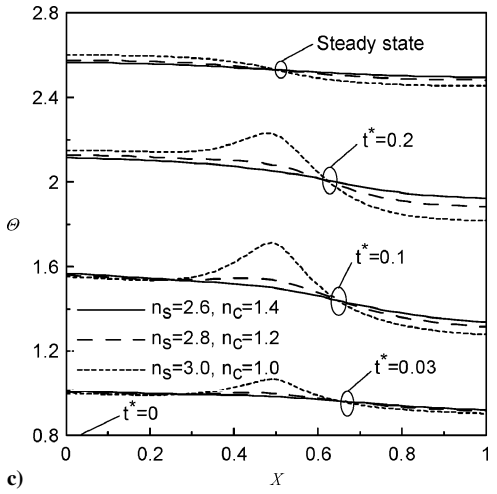

Fig. 6 Effects of different optical thickness on transient temperature fields: a) $\tau = 0.05$, b) $\tau = 0.25$, c) $\tau = 0.5$.

the peaks turn more and more obvious. At steady state, the temperature peaks disappear completely and three temperature profiles are almost superposed with each other. As optical thickness increases, temperature profiles become sloped from the left down to the right, as shown in Figs. 6b and 6c, and the peaks will disappear if the optical thickness is great enough. In the case of $n(X) = 2.6–1.2\sin(\pi X)$, there is no temperature peak when $\tau = 0.25$, and in the case of $n(X) = 2.8–1.6\sin(\pi X)$, the temperature peak does not exist when $\tau = 0.5$. When the optical thickness is great enough, we can infer that the temperature peak for $n(X) = 3.0–2.0\sin(\pi X)$ will also disappear. The reasons are that, on the one hand, the greater the optical thickness is, the stronger absorption of the radiative energy is in outer region close to the left surface, and the weaker absorption of

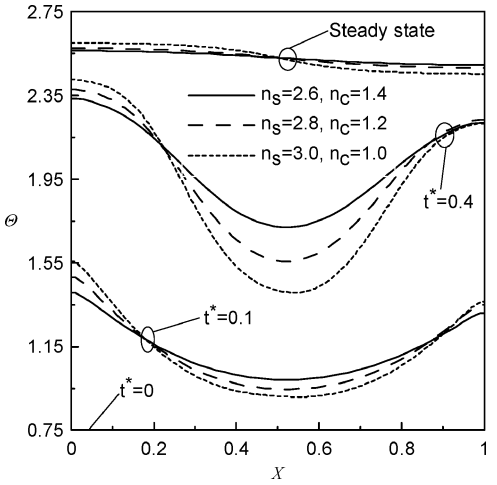

Fig. 7 Transient temperature distributions in strong scattering medium with $\omega = 0.9$ for $\tau = 0.5$.

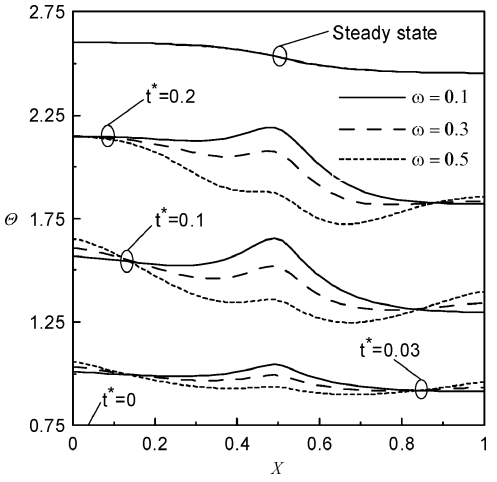

Fig. 8 Effect of scattering albedo on the transient temperature distributions with $n(X) = 3.0 - 2.0\sin(\pi X)$ for $\tau = 0.5$.

the radiative energy is in center region and in outer region close to the right surface; on the other hand, weaker thermal emission cause inner regions to have larger absorbency of the radiative energy. Therefore, under the two effects, if absorbency of the energy is dominant therein, temperature peak will appear, and if absorbency of the energy is not dominant, there will be no temperature peak appearing therein.

With Fig. 6c as a reference, Figs. 7 and 8 display a heavy effect of scattering on transient temperature distributions. For the same refractive index distributions and parameters, except for ω used in Fig. 6c, the curves of transient temperature distributions in Fig. 7 are similar to those of refractive index distributions; that is, temperature maximum appears at surfaces and minimal temperature is in middle areas. Scattering must deviate some rays that would normally be reflected, to directions where they are actually transmitted. On the other hand, assuming the scattering albedo to 0.9 and the extinction coefficient constant, as is done in Fig. 7, the thermal emission within the medium is dramatically reduced, and the transient temperature distributions are quite different from the case of $\omega = 0$, where high temperature appears at regions having a high refractive index, and low temperature exists in areas of a low refractive index. According to above analysis, compared with the case of $\omega = 0$, scattering effects can cause regions having a higher refractive index to absorb more energy, and can cause regions having a lower refractive index to absorb less energy. As a result, scattering can redistribute radiative energy through the slab, compared with Fig. 6c, where nonscattering is considered. Especially for the case of a high scattering albedo, the effect of energy redistribution is very obvious, whereas for the case of a low scattering albedo, $\omega = 0.1$, as shown in Fig. 8, scattering

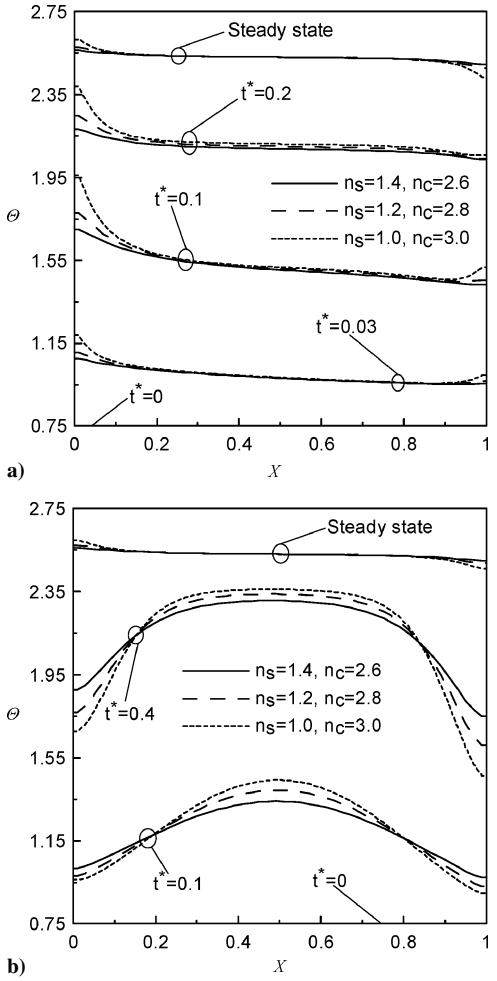

Fig. 9 Transient temperature distributions in sinusoidal refractive index medium with $n_s < n_c$ for $\tau = 0.5$: a) $\omega = 0$ and b) $\omega = 0.9$.

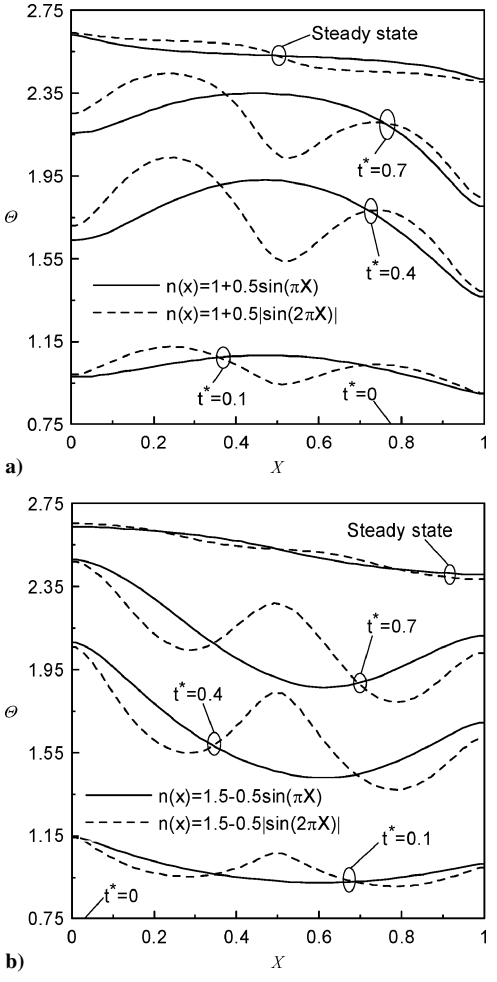

Fig. 10 Effects of different refractive index distribution on temperature peaks in strong scattering medium with $\omega = 0.9$ for $\tau = 0.5$.

effect is not dominant, so the transient temperature fields are still similar to those of the case where $\omega = 0$. However, as scattering albedo increases, influence of the scattering increases. If scattering albedo is so high that transient temperature fields are mainly affected by scattering, the maximum temperature will disappear in inner regions and appear at boundaries for the case of $n_s > n_c$, as shown in temperature profiles for $\omega = 0.5$ of Fig. 8.

For the case of $n_s < n_c$, thermal emissive power in outer regions is weaker than that in inner regions. In a slab having $\omega = 0$, outer regions will absorb more radiative energy than inner regions. This causes maximum temperature to appear not at the center of the slab but at the left boundary, as shown in Fig. 9a. In Fig. 9b, due to strong scattering, transient temperature distributions are quite different from that in Fig. 9a, where $\omega = 0$: temperature peaks appear at the center of the slab instead of at boundary surfaces.

Effect of a refractive index distribution on temperature peaks in a strong scattering slab having $\omega = 0.9$ is plotted in Fig. 10. From Fig. 10a we can see that there are two temperature peaks in inner regions for $n(X) = 1 + 0.5|\sin(2\pi X)|$ and one peak for $n(X) = 1 + 0.5\sin(\pi X)$. This can be explained qualitatively as follows: $n(X)$ has two maximal in inner regions where thermal emission is most intensive, and due to strong scattering, more energy will be absorbed therein, which is quite different from the case of $\omega = 0$. Figure 10b presents transient temperature profiles for $n(X) = 1.5 - 0.5\sin(\pi X)$ and $n(X) = 1.5 - 0.5|\sin(2\pi X)|$, and we can also explain the transient temperature distributions in the slab by a similar qualitative analysis.

From Figs. 6–10, we can see that temperature peaks or minimum temperatures in a GRIN slab appear only in transient coupled heat transfer and do not exist at steady state.

Conclusions

Using a ray-tracing technique based on a zonal method, a multilayer radiative transfer model of specular reflection is established to simulate radiative transfer in a GRIN slab. By a node analysis, radiative source term is obtained with the assistance of RTCs deduced by the multilayer radiative transfer model and considering isotropic scattering, and transient coupled radiative–conductive heat transfer inside a nonlinearly varying refractive index distribution scattering slab having specular semitransparent boundary surfaces is solved. Results of this paper are also compared with published results and main conclusions can be drawn as follows:

1) Comparisons of results with those of Refs. 27 and 34 show that the multilayer simulation of radiative transfer in a graded refractive index slab is correct and reliable at radiative conductive coupling and radiative equilibrium, respectively.

2) A temperature peak also appears in inner regions of an absorbing–emitting medium having both semitransparent surfaces and subjected to external radiation without convection at both boundaries even though the medium absorption coefficient is spatially uniform for the case $n(X) = n_s + (n_c - n_s)\sin(\pi X)$ where $n_s > n_c$; and with increasing of absorption coefficient, the temperature peak gradually becomes inconspicuous until it disappears.

3) Transient temperature distributions within a strongly scattering medium are quite different from that of $\omega = 0$ due to scattering, which can redistribute radiative energy. Therefore, in a strongly scattering medium having a refractive index distribution of $n(X) = n_s + (n_c - n_s)\sin(\pi X)$, where $n_s > n_c$, a maximal temperature appears at boundaries and a minimal temperature appears in inner regions, whereas for $n_s < n_c$, a temperature peak appears again in inner regions under the conditions considered in this paper.

4) Temperature peaks in a graded refractive index medium, mainly caused by low thermal emission for the case of $\omega = 0$ and by strong scattering for the case of high albedo, appear only in the transient state, and at steady state, under the parameters for calculations given in this paper, temperature peaks disappear in inner regions of the medium no matter consider scattering or not.

Acknowledgments

This research is supported by a key project of the National Natural Science Foundation of China (Grant 50336010) and by the China National Key Basic Research Special Funds (Grant 2003CB214500). The authors are indebted to them for their financial support.

References

[1]Frankel, J. I., "Cumulative Variable Formulation for Transient Conductive and Radiative Transport in Participating Medium," *Journal of Thermophysics and Heat Transfer*, Vol. 9, No. 2, 1995, pp. 210–218.

[2]Abulwafa, E. M., "Conductive–Radiative Heat Transfer in an Inhomogeneous Slab with Directional Raflecting Boundaries," *Journal of Physics D: Applied Physics*, Vol. 32, No. 14, 1999, pp. 1626–1632.

[3]Vilhena, M. T., Thompson, M., Pazos, R. P., and Ourique, L. E., "Qualitative Analysis of the S_N Approximations of the Transport Equation and Combined Conduction–Radiation Heat Transfer Problem," *Progress in Nuclear Energy*, Vol. 42, No. 4, 2003, pp. 427–437.

[4]Muresan, C., Vaillon, R., Menezo, C., and Morlot, R., "Discrete Ordinates Solution of Coupled Conductive Radiative Heat Transfer in a Two-Layer Slab with Fresnel Interfaces Subject to Diffuse and Obliquely Collimated Irradiation," *Journal of Quantitative Spectroscopy and Radiative Transfer*, Vol. 84, No. 4, 2004, pp. 551–562.

[5]Tan, H. P., Wang, P. Y., and Xia, X. L., "Transient Coupled Radiation and Conduction in an Absorbing and Scattering Composite Layer," *Journal of Thermophysics and Heat Transfer*, Vol. 14, No. 1, 2000, pp. 77–87.

[6]Tan, H. P., Luo, J. F., and Xia, X. L., "Transient Coupled Radiation and Conduction in a Three-Layer Composite with Semitransparent Specular Interfaces and Surfaces," *Journal of Heat Transfer*, Vol. 124, No. 2, 2002, pp. 470–481.

[7]Tsai, C. F., and Nixon, G., "Transient Temperature Distribution of a Multilayer Composite Wall with Effects of Internal Radiation and Conduction," *Numerical Heat Transfer*, Vol. 10, No. 1, 1986, pp. 95–101.

[8]Timoshenko, V. P., and Trenev, M. G., "A Method for Evaluation Heat Transfer in Multilayer Semitransparent Materials," *Heat Transfer-Soviet Research*, Vol. 18, No. 5, 1986, pp. 44–57.

[9]Luo, J. F., Tan, H. P., Ruan, L. M., and Tong, T. W., "Refractive Index Effects on Heat Transfer in Multilayer Scattering Composite," *Journal of Thermophysics and Heat Transfer*, Vol. 17, No. 3, 2003, pp. 407–419.

[10]Siegel, R., "Transient Thermal Effects of Radiant Energy in Translucent Materials," *Journal of Heat Transfer*, Vol. 120, No. 1, 1998, pp. 4–23.

[11]Siegel, R., and Spuckler, C. M., "Variable Refractive Index Effects on Radiation in Semitransparent Scattering Multilayered Regions," *Journal of Thermophysics and Heat Transfer*, Vol. 7, No. 4, 1993, pp. 624–630.

[12]Siegel, R., and Spuckler, C. M., "Refractive Index Effects on Radiation in an Absorbing, Emitting, and Scattering Laminated Layer," *Journal of Heat Transfer*, Vol. 115, No. 1, 1993, pp. 194–200.

[13]Spuckler, C. M., and Siegel, R., "Refractive Index Effects on Radiative Behavior of a Heated Absorbing–Emitting Layer," *Journal of Thermophysics and Heat Transfer*, Vol. 6, No. 4, 1992, pp. 596–604.

[14]Siegel, R., "Refractive Index Effects on Transient Cooling of a Semitransparent Radiating Layer," *Journal of Thermophysics and Heat Transfer*, Vol. 9, No. 1, 1995, pp. 55–62.

[15]Siegel, R., "Transient Thermal Analysis of Parallel Translucent Layers by Using Green's Functions," *Journal of Thermophysics and Heat Transfer*, Vol. 13, No. 1, 1999, pp. 10–17.

[16]Liu, C. C., and Dougherty, R. L., "Anisotropically Scattering Media Having a Reflective Upper Boundary," *Journal of Thermophysics and Heat Transfer*, Vol. 13, No. 2, 1999, pp. 177–184.

[17]Crosbie, A. L., and Shieh, S. M., "Three-Dimensional Radiative Transfer for Anisotropic Scattering Medium with Refractive Index Greater Than Unity," *Journal of Quantitative Spectroscopy and Radiative Transfer*, Vol. 44, No. 2, 1990, pp. 299–312.

[18]Schwander, D., Flamant, G., and Olalde, G., "Effects of Boundary Properties on Transient Temperature Distributions in Condensed Semitransparent Media," *International Journal of Heat and Mass Transfer*, Vol. 33, No. 8, 1990, pp. 1685–1695.

[19]Su, M. H., and Sutton, W. H., "Transient Conductive and Radiative Heat Transfer in a Silica Window," *Journal of Thermophysics and Heat Transfer*, Vol. 9, No. 2, 1995, pp. 370–373.

[20]Siegel, R., and Spuckler, C. M., "Effects of Refractive Index and Diffuse or Specular Boundaries on a Radiating Isothermal Layer," *Journal of Heat Transfer*, Vol. 116, No. 3, 1994, pp. 787–790.

[21]Luo, J. F., Xia, X. L., Tan, H. P., and Tong, T. W., "Transient Coupled Heat Transfer in Three-Layer Composite with Opaque Specular Surfaces," *Journal of Thermophysics and Heat Transfer*, Vol. 16, No. 3, 2002, pp. 297–305.

[22]Ben Abdallah, P., and Le Dez, V., "Temperature Field Inside an Absorbing–Emitting Semitransparent Slab at Radiative Equilibrium with Variable Spatial Refractive Index," *Journal of Quantitative Spectroscopy and Radiative Transfer*, Vol. 65, No. 4, 2000, pp. 595–608.

[23]Ben Abdallah, P., and Le Dez, V., "Radiative flux Field inside an Absorbing-Emitting Semitransparent Slab with Variable Spatial Refractive Index at Radiative Conductive Coupling," *Journal of Quantitative Spectroscopy and Radiative Transfer*, Vol. 67, No. 2, 2000, pp. 125–137.

[24]Lemonnier, D., and Le Dez, V., "Discrete Ordinates Solution of Radiative Transfer across a Slab with Variable Refractive Index," *Journal of Quantitative Spectroscopy and Radiative Transfer*, Vol. 73, No. 2, 2002, pp. 195–204.

[25]Huang, Y., Xia, X. L., and Tan, H. P., "Temperature Field of Radiative Equilibrium in a Semitransparent Slab with a Linear Refractive Index and Gray Walls," *Journal of Quantitative Spectroscopy and Radiative Transfer*, Vol. 74, No. 2, 2002, pp. 249–261.

[26]Xia, X. L., Huang, Y., and Tan, H. P., "Simultaneous Radiation and Conduction Heat Transfer in a Graded Index Semitransparent Slab with Gray Boundaries," *International Journal of Heat and Mass Transfer*, Vol. 45, No. 13, 2002, pp. 2673–2688.

[27]Huang, Y., Xia, X. L., and Tan, H. P., "Radiation Equilibrium Temperature Field in a Gradient Index Medium with Specular Surfaces," *Heat and Mass Transfer*, Vol. 39, No. 10, 2003, pp. 835–842.

[28]Liu, L. H., "Discrete Curved Ray-Tracing Method for Radiative Transfer in an Absorbing–Emitting Semitransparent Slab with Variable Spatial Refractive Index," *Journal of Quantitative Spectroscopy and Radiative Transfer*, Vol. 83, No. 2, 2004, pp. 223–228.

[29]Liu, L. H., Zhang, H. C., and Tan, H. P., "Monte Carlo Discrete Curved Ray-Tracing Method for Radiative Transfer in an Absorbing–Emitting Semitransparent Slab with Variable Spatial Refractive Index," *Journal of Quantitative Spectroscopy and Radiative Transfer*, Vol. 84, No. 3, 2004, pp. 357–362.

[30]Ben Abdallah, P., Fumeron, S., Le Dez, V., and Charette, A., "Integral Form of the Radiative Transfer Equation Inside Refractive Cylindrical Media," *Journal of Thermophysics and Heat Transfer*, Vol. 15, No. 2, 2001, pp. 184–189.

[31]Ben Abdallah, P., Le Dez, V., Lemonnier, D., Fumeron, S., and Charette, A., "Inhomogeneous Radiative Model of Refractive and Dispersive Semitransparent Stellar Atmospheres," *Journal of Quantitative Spectroscopy and Radiative Transfer*, Vol. 69, No. 1, 2001, pp. 61–80.

[32]Liu, L. H., Tan, H. P., and Yu, Q. Z., "Temperature Distributions in an Absorbing–Emitting–Scattering Semitransparent Slab with Variable Spatial Refractive Index," *International Journal of Heat and Mass Transfer*, Vol. 46, No. 15, 2003, pp. 2917–2920.

[33]Huang, Y., Liang, X. G., and Xia, X. L., "Monte Carlo Simulation of Radiative Transfer in Scattering, Emitting, Absorbing Slab with Gradient Index," *Journal of Quantitative Spectroscopy and Radiative Transfer*, Vol. 92, No. 1, 2005, pp. 111–120.

[34]Huang, Y., Xia, X. L., and Tan, H. P., "Coupled Radiation and Conduction in a Graded Index Layer with Specular Surfaces," *Journal of Thermophysics and Heat Transfer*, Vol. 18, No. 2, 2004, pp. 281–285.

[35]Liu, L. H., and Tan, H. P., "Transient Temperature Response in Semitransparent Variable Refractive Index Medium Subjected to a Pulse Irradiation," *Journal of Quantitative Spectroscopy and Radiative Transfer*, Vol. 83, No. 3–4, 2004, pp. 333–344.

[36]Tan, H. P., Luo, J. F., Ruan, L. M., and Yu, Q. Z., "Transient Coupled Heat Transfer in a Multi-Layer Composite with Opaque Specular Surfaces and Semitransparent Specular Interfaces," *International Journal of Thermal Sciences*, Vol. 42, No. 2, 2003, pp. 209–222.

[37]Tan, H. P., Yi, H. L., Zhang H. C., Wang P. Y., and Tong, T. W., "Coupled Radiation–Conduction Heat Transfer in an Anisotropically Scattering Slab with Mixed Boundaries," *Journal of Quantitative Spectroscopy and Radiative Transfer*, Vol. 83, No. 3–4, 2004, pp. 667–698.

[38]Hottel, H. C., and Sarofim, A. F., *Radiative Transfer*, McGraw–Hill, New York, 1967, pp. 265–266.

[39]Goyhénèche, J. M., and Sacadura, J. F., "The Zone Method: A New Explicit Matrix Relation to Calculate the Total Exchange Areas in Anisotropically Scattering Medium Bounded by Anisotropically Reflecting Walls," *Journal of Heat Transfer*, Vol. 124, No. 4, 2002, pp. 696–703.

[40]Tan, H. P., and Yu, Q. Z., "Numerical Analysis of Temperature Field in Materials During Infrared Heating," *Chinese Journal of Infrared and Millimeter Waves*, 10, No. 2, 1991, pp. 169–178.